Electronic structure and magnetic exchange coupling in ferromagnetic full Heusler alloys

Yasemin Kurtulus and Richard Dronskowski
Institut für Anorganische Chemie, Rheinisch-Westfälische Technische Hochschule, 52056 Aachen, Germany

German D. Samolyuk and Vladimir P. Antropov
Condensed Matter Physics, Ames Laboratory, Ames, Iowa 50011, USA
(Received 21 June 2004; revised manuscript received 23 September 2004; published 19 January 2005)

Density-functional studies of the electronic structures and exchange interaction parameters have been performed for a series of ferromagnetic full Heusler alloys of general formula Co_2MnZ (Z=Ga, Si, Ge, Sn), Rh_2MnZ (Z=Ge, Sn, Pb), Ni_2MnSn, Cu_2MnSn, and Pd_2MnSn, and the connection between the electronic spectra and the magnetic interactions have been studied. Different mechanisms contributing to the exchange coupling are revealed. The band dependence of the exchange parameters, their dependence on volume and valence electron concentration have been thoroughly analyzed within the Green function technique. The difference between the exact adiabatic approach and the long-wavelength approximation is discussed.

DOI: 10.1103/PhysRevB.71.014425 PACS number(s): 75.50.Cc, 71.15.Mb, 71.20.Lp

I. INTRODUCTION

The evolving field of spin-electronics has triggered an increasing interest in materials with full spin polarization at the Fermi level. Many of these systems have been predicted by means of electronic band-structure calculations,[1,2] and some of them are in use already as elements in multilayered magnetoelectronic devices such as magnetic tunnel junctions[3,4] and also as giant magnetoresistance spin valves.[5] Promising device candidates are characterized by a strong spin polarization, by a high Curie temperature (T_C) and by a large band gap, too. Among the most popular groups of materials is the extraordinarily large family of magnetic Heusler alloys[6] which is traditionally considered to be an ideal local-moment system.[7–9] This implies that their exchange couplings can be described by a Heisenberg Hamiltonian which allows the investigation of the temperature properties of the magnetic systems within a very simple conceptual frame. It therefore seems that the problem of calculating the exchange interaction parameters with the help of reliable electronic structure methods must have a very high priority in this field.

Nonetheless, despite a thorough theoretical understanding of the electronic structures of many full Heusler alloys (see, for example, Refs. 9–15), only very few publications are dedicated to the discussions of magnetic exchange interactions in these systems. Noda and Ishikawa[16] have extracted the exchange parameters from the spin-wave spectrum using a model-like Heisenberg fit. On the theoretical side, Kübler, Williams, and Sommers focused on the calculated total-energy differences between the ferromagnetic (FM) and different antiferromagnetic (AFM) states.[9] The parameters of the Heisenberg Hamiltonian were then fitted to reproduce the course of the calculated energies but such technique usually allows to extract only the parameters of the first and second neighbors, and the interactions between Mn and all other atoms are neglected for reasons of simplicity.

In this contribution, we obtain the magnetic exchange parameters of a number of Heusler alloys from first principles and then analyze the magnetic coupling dependence upon electronic structure variations induced by atomic substitutions or volume variations. The paper is organized as follows: In Sec. II we describe the crystal structure under investigation and the computational method chosen. Section III is devoted to the parameter-free derivation of exchange parameters by theoretical approaches within density-functional theory. Section IV contains our results for the electronic structures and the magnetic interaction parameters of the Co_2MnZ, Rh_2MnZ and X_2MnSn families of alloys. Finally, we summarize our results in Sec. V.

II. CRYSTAL STRUCTURE AND COMPUTATIONAL DETAILS

The Heusler alloys[6] represent a class of ternary intermetallic compounds of general formula X_2YZ in which X is a transition metal, Z is a metal of main groups III-V, and Y is a magnetically active transition metal such as manganese. The Heusler alloys adopt ordered $L2_1$ structures, given in Fig. 1, which may be understood as being the result of four interpenetrating face-centered-cubic (fcc) lattices. According to the $L2_1$ structure jargon, the X atoms occupy the A and C sites, the Y atoms are on the B sites, and the Z atoms are found on the D sites. Thus, sites A, B, C and D correspond to

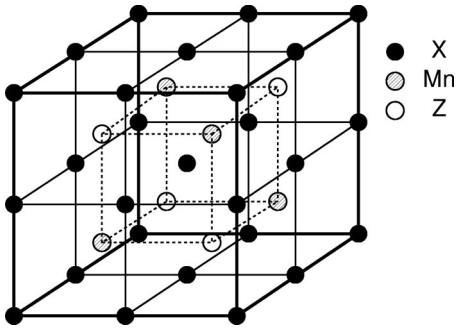

FIG. 1. The $L2_1$ structure type composed of four interpenetrating fcc lattices.

TABLE I. Experimental lattice parameters a, calculated partial and experimental total magnetic moments μ, and calculated and experimental Curie temperatures T_C for X_2MnZ compounds. All experimental values have been taken from Ref. 35.

		$\mu_{\text{calc}}(\mu_B)$			$\mu_{\text{expt}}(\mu_B)$	T_C (K)		
Compound	a (a.u.)	X	Mn	Total	Total	LWA	Exact	Expt.
Co_2MnGa	10.904	0.73	2.78	4.13	4.05	635	807	694
Co_2MnSi	10.685	1.01	3.08	5.00	5.07	1251	1434	985
Co_2MnGe	10.853	0.97	3.14	5.00	5.11	1115	1299	905
Co_2MnSn	11.338	0.95	3.24	5.04	5.08	1063	1215	829
Rh_2MnGe	11.325	0.42	3.67	4.49	4.62	410	504	450
Rh_2MnSn	11.815	0.45	3.73	4.60	3.10	435	537	412
Rh_2MnPb	11.966	0.45	3.69	4.58	4.12	423	530	338
Ni_2MnSn	11.439	0.23	3.57	3.97	4.05	373	461	344
Cu_2MnSn	11.665	0.04	3.79	3.81	4.11	602	624	530
Pd_2MnSn	12.056	0.07	4.02	4.07	4.23	232	254	189

the positions (0,0,0), $(\frac{1}{4},\frac{1}{4},\frac{1}{4})$, $(\frac{1}{2},\frac{1}{2},\frac{1}{2})$ and $(\frac{3}{4},\frac{3}{4},\frac{3}{4})$ within the fcc supercell.[17]

The uniqueness of the Heusler alloys is due to the fact that they exhibit cooperative magnetic phenomena—especially ferromagnetism—in the desired temperature range although no constituent of their archetype, Cu_2MnAl, exhibits such properties in the elemental state. Even simpler than Cu_2MnAl is the phase MnAl which also displays strong ferromagnetic behavior and is of technological interest because of an enhanced magnetic anisotropy. The tetragonal MnAl ground state results from two subsequent (electronic and structural) distortions away from a cubic structure.[18] The group of cubic Heusler alloys considered in this paper, however, all contain Mn atoms as the Y atoms, and all phases exhibit ferromagnetic order. Their lattice parameters, magnetic saturation moments and also experimental Curie temperatures are shown in Table I.

For the band-structure calculation we used the TB-LMTO-ASA method[19,20] and took the experimental values of the lattice parameters. The local density approximation (LDA) according to the Vosko-Wilk-Nusair exchange-correlation functional was used.[21] The tetrahedron integration over the entire Brillouin zone (BZ) was performed with a total of 195 **k** points in the irreducible part of the BZ. The Green function technique was implemented according to Ref. 22.

III. THE CALCULATION OF EXCHANGE-INTERACTIONS PARAMETERS IN DENSITY-FUNCTIONAL THEORY

In this paper we will use a linear-response technique for the calculation of the exchange coupling. This technique was first applied for the description of the exchange coupling between magnetic impurities in diluted alloys and is traditionally required for the so-called Ruderman-Kasuya-Kittel-Yosida (RKKY) interaction.[23] While the formalism was successful for many systems (diluted magnetic alloys, f magnets, spin glasses, etc.), such a perturbative treatment is not applicable for systems with strong interatomic exchange couplings, and it is valid only asymptotically ($\mathbf{R}\rightarrow\infty$). Surprisingly enough, the case of a strong exchange coupling was never analyzed in the theory of magnetism for real materials but the so-called long-wave approximation (LWA) was considered, for many years, as the suitable approach in the density-functional community. Recently, we reconsidered the most general definition of the exchange coupling and analyzed several conditions of LWA applicability.[24] Below we will apply both "exact" and LWA adiabatic formalisms for the calculation of J_{ij} in Heusler alloys where both localized and itinerant types of magnetism coexist. First we shortly describe our computational approach.

The exchange coupling parameter J_{ij} between two centers i and j being part of a magnetic material is usually defined in the following standard adiabatic procedure using the so-called rigid spin approximation (RSA),[24]

$$J_{ij} = \mathbf{m}_i \frac{\partial^2 E}{\partial \mathbf{m}_i \, \partial \mathbf{m}_j} \mathbf{m}_j = \mathbf{m}_i [\chi]^{-1}_{ij} \mathbf{m}_j, \tag{1}$$

where E is the total energy of the system, $\mathbf{m}_i$ is the magnetic moment on site i, and χ_{ij} is a static magnetic susceptibility.

In the above Eq. (1), the entry χ can also be formulated as the adiabatic (static) limit ($\omega\rightarrow 0$) of the transversal part of the Fourier transform of the **q**-dependent transversal part of the spin-dynamical susceptibility

$$\chi(\mathbf{q},\omega) = \sum \frac{\varphi^{\uparrow}_{\nu}(\mathbf{k}) \varphi^{*\downarrow}_{\nu'}(\mathbf{k}+\mathbf{q}) \varphi^{*\uparrow}_{\nu}(\mathbf{k}) \varphi^{\downarrow}_{\nu'}(\mathbf{k}+\mathbf{q})}{\varepsilon^{\uparrow}_{\nu}(\mathbf{k}) - \varepsilon^{\downarrow}_{\nu'}(\mathbf{k}+\mathbf{q}) - \omega + i0}, \tag{2}$$

where $\varphi^{\uparrow}_{\nu}(\mathbf{k})$ and $\varepsilon^{\uparrow}_{\nu}(\mathbf{k})$ are eigenfunctions and eigenvalues of the band-structure problem, and the arrows designate different spin directions. It can be shown that the static limit of this susceptibility contributes to the adiabatic full-potential expression for the spin-wave spectrum[25,26]

$$\omega(\mathbf{q}) = m\{[\chi(\mathbf{q})]^{-1}K_{\mathbf{q}} - [\chi(0)]^{-1}\}, \quad (3)$$

where the Fourier transform of $K_{\mathbf{q}}$ is

$$K(\mathbf{r},\mathbf{r}') = 1 - \sum \frac{f_{\nu'\uparrow} - f_{\nu\downarrow}}{\varepsilon_{\nu}^{\uparrow} - \varepsilon_{\nu'}^{\downarrow} + i0}\varphi_{\nu'}^{*\uparrow}(\mathbf{r})\varphi_{\nu}^{\downarrow}(\mathbf{r})\,\nabla \times\Big[\varphi_{\nu'}^{\uparrow}(\mathbf{r}')\,\nabla\,\varphi_{\nu}^{*\downarrow}(\mathbf{r}') - \varphi_{\nu}^{*\downarrow}(\mathbf{r}')\,\nabla\,\varphi_{\nu'}^{\uparrow}(\mathbf{r}')\Big], \quad (4)$$

and $f_{\nu\uparrow}$ is a Fermi function. Equation (4) describes the difference in the spatial distribution of the wave functions for the different spins and is negligible if the spin full-potential effects are small or if the spatial dispersions of the bands with different spins are the same. Assuming $K_{\mathbf{q}}=1$ (very small effects of the "kinetic" exchange or large $B_{\mathrm{xc}}=\varepsilon_{\nu}^{\uparrow} - \varepsilon_{\nu'}^{\downarrow}$, where B_{xc} is the exchange-correlation field), the well-known Heisenberg-type dispersion law is obtained

$$\omega(\mathbf{q}) = m[\chi^{-1}(\mathbf{q}) - \chi^{-1}(0)] = m[J(\mathbf{q}) - J(0)]. \quad (5)$$

The static (adiabatic) limit used above can be justified if

$$\varepsilon_{\nu}^{\uparrow}(\mathbf{k}) - \varepsilon_{\nu'}^{\downarrow}(\mathbf{k}+\mathbf{q}) \approx Im \gg \omega, \quad (6)$$

where I is an effective Stoner parameter and $m=|\mathbf{m}|$. This condition [Eq. (6)] determines a whole range of spin-wave frequencies for which one may use the adiabatic approximation.

Below we will estimate the validity of the above criterion for several compounds studied in this paper. Whenever Eq. (6) is satisfied in localized systems, however, Eq. (1) can be further simplified if the LWA is applied using a smallness criteria either in reciprocal space,

$$[\chi^{-1}(\mathbf{q}) - \chi^{-1}(0)]/\chi^{-1}(0) \ll 1, \quad (7)$$

or in real space,

$$\chi_{ij}^{-1}/\chi_{ii}^{-1} \approx J_{ij}/I_i \ll 1. \quad (8)$$

Then, the exchange coupling in the LWA can be expressed as

$$J_{ij}^{\mathrm{lw}} = \mathbf{m}_i[\chi]_{ij}^{-1}\mathbf{m}_j \approx \mathbf{m}_i\chi_i^{-1}\chi_{ij}\chi_j^{-1}\mathbf{m}_j \approx \mathbf{m}_i I_i\chi_{ij}I_j\mathbf{m}_j, \quad (9)$$

where χ_i^{-1} is the on-site element of the inverted spin susceptibility. Due to similarity between Eq. (6) and Eqs. (7) and (8), one cannot use the static (adiabatic) expression [Eq. (5) or any type of Heisenberg model] for large $\mathbf{q}$ values if requirement (7) is fulfilled. The model will be correct for both itinerant and localized systems for short spin wavelengths (large $\mathbf{q}$) only if *both* the LWA and the adiabatic approximation are removed simultaneously.

The currently most practical expression for the exchange coupling is based on the Green function or multiple-scattering formalism. In this technique, an analogue of Eq. (1) can be derived[24] which reads

$$\begin{aligned} J(\mathbf{q}) &= \frac{1}{N}\sum J_{ij}e^{i\mathbf{q}\mathbf{R}_{ij}} \\ &= \frac{1}{N}\sum \frac{1}{\pi}\int^{E_F} d\varepsilon\,\mathrm{Im\,Tr}\{\Delta_i[T^{\uparrow}T^{\downarrow}]_{ij}^{-1}\Delta_j\}e^{i\mathbf{q}\mathbf{R}_{ij}} \\ &= \frac{1}{\pi}\int^{E_F} d\varepsilon\,\mathrm{Im\,Tr}\left[\Delta_i\left(\int d\mathbf{k}T^{\uparrow}(\mathbf{k})T^{\downarrow}(\mathbf{k}+\mathbf{q})\right)^{-1}\Delta_i\right], \end{aligned} \quad (10)$$

where $\Delta_i=(T_{ii}^{\uparrow}-T_{ii}^{\downarrow})/2$ and

$$T_{ij}^{\sigma} = \frac{1}{\Omega_{BZ}}\int d\mathbf{k}T^{\sigma}(\mathbf{q})e^{i\mathbf{q}\mathbf{R}_{ij}} = \frac{1}{\Omega_{BZ}}\int d\mathbf{k}[p^{\sigma}(\varepsilon) - S(\mathbf{q})]^{-1}e^{i\mathbf{q}\mathbf{R}_{ij}}. \quad (11)$$

Here, T^{σ} is a scattering path operator, $p^{\sigma}(\varepsilon)$ is an atomic-potential scattering matrix and S is a matrix of structure constants. The corresponding LWA $J^{\mathrm{lw}}(\mathbf{q})$ was obtained in Ref. 27 and reads

$$J^{\mathrm{lw}}(\mathbf{q}) = \frac{1}{\pi\Omega_{BZ}}\int^{E_F}\int d\mathbf{k}d\varepsilon\,\mathrm{Im\,Tr}\{pT^{\uparrow}(\mathbf{k})T^{\downarrow}(\mathbf{k}+\mathbf{q})p\}, \quad (12)$$

where $p=(p^{\uparrow}-p^{\downarrow})/2$. In real space, the zero-moment of the exchange interactions can be calculated accordingly to the sum rule

$$J_i^{\mathrm{lw}} = \sum_{j\neq i} J_{ij}^{\mathrm{lw}} = \frac{1}{\pi}\int^{E_F} d\varepsilon\,\mathrm{Im\,Tr}\left(p_i\Delta_i + p_iT_i^{\uparrow}T_i^{\downarrow}p_i\right). \quad (13)$$

The linearization of the multiple-scattering expression leads to the LMTO Green function formalism where, in a two-center approximation, the T^{σ} matrix can be replaced by its linearized analogue

$$T_{ij}^{\sigma}(\varepsilon) = \Delta^{1/2}G_{ij}^{\sigma}\Delta^{1/2}, \quad (14)$$

where G_{ij}^{σ} is the pairwise LMTO Green function, and the spin-dependent LMTO potential parameter Δ^{σ} is a bandwidth for a given quantum number. The LMTO linearization represents a well-known low-energy scattering in quantum mechanics, and a potential scattering function can be presented as

$$p^{\sigma}(\varepsilon) = \frac{C^{\sigma}-\varepsilon}{\Delta^{\sigma}}, \quad (15)$$

where the parameter C^{σ} is the center of a band. One can show[28] that in this approximation the effective exchange can be presented as

$$\begin{aligned} J_{ij}^{\mathrm{lw}} &= \frac{1}{\pi}\int^{E_F} d\varepsilon\,\mathrm{Im\,Tr}\left\{\left[C^{\uparrow}\left(\frac{\Delta^{\downarrow}}{\Delta^{\uparrow}}\right)^{1/2} - C^{\downarrow}\left(\frac{\Delta^{\uparrow}}{\Delta^{\downarrow}}\right)^{1/2}\right]\right. \\ &\quad \left.\times G_{ij}^{\uparrow}G_{ji}^{\downarrow}\left[C^{\uparrow}\left(\frac{\Delta^{\downarrow}}{\Delta^{\uparrow}}\right)^{1/2} - C^{\downarrow}\left(\frac{\Delta^{\uparrow}}{\Delta^{\downarrow}}\right)^{1/2}\right]\right\} \\ &= \frac{1}{\pi}\mathrm{Im\,Tr}\,V_i\left(\int^{E_F} d\varepsilon G_{ij}^{\uparrow}G_{ji}^{\downarrow}\right)V_j = \mathrm{Tr}\,V_i\chi_{ij}V_j, \end{aligned} \quad (16)$$

where $V=C^{\uparrow}(\Delta^{\downarrow}/\Delta^{\uparrow})^{1/2}-C^{\downarrow}(\Delta^{\uparrow}/\Delta^{\downarrow})^{1/2}$ is the effective spin splitting. So, whenever $\Delta^{\uparrow}=\Delta^{\downarrow}$, that is, equal bandwidth for different spin projections, then $V=C^{\uparrow}-C^{\downarrow}=Im$, and the Fourier transform of Eq. (12) can be rewritten in the form of Eq. (9). It is this limiting case which allows us to separate the pure Stoner splitting and hybridization (different bandwidths for different spin bands) contributions from the total exchange coupling. In the present paper, we will mostly use the Fourier transform of Eq. (12) because of its simplicity, but the applicability of this approach will be checked and Eq. (10) will be used if necessary. A significant difference between these two approaches would indicate that the adiabatic (or LWA) criterion [Eq. (6)] is not fulfilled and the nonadiabatic corrections should be added. To avoid any further complications, we will be using the simple mean field approximation (MFA) for the T_C estimation below.

Due to the presence of several magnetic atoms in a primitive cell, a multiatomic expression for T_C must be used. In the MFA, T_C of a system with N nonequivalent magnetic atoms is calculated[29] as a largest solution of the equation

$$\det(T_{nm}-T\delta_{nm})=0, \tag{17}$$

where n and m are the indices of the nonequivalent magnetic sublattices, $T_{nm}=\frac{2}{3}J^0_{mn}$, and J^0_{mn} is an effective interaction of an atom from sublattice n with all other atoms from the sublattice m. In our case with two nonequivalent magnetic atoms per cell, the expression for T_C is reduced to

$$T_C=\tfrac{1}{3}[J^0_{\text{Mn-Mn}}+J^0_{X\text{-}X}+\sqrt{(J^0_{\text{Mn-Mn}}-J^0_{X\text{-}X})^2+4(J^0_{\text{Mn-}X})^2}]. \tag{18}$$

While below we provide the MFA estimation of T_C using both approaches described above, a significant difference between J_{ij} and J^{lw}_{ij} may indicate the presence of some magnetic short-range order or a large degree of itineracy in the system.[36] In this case, such a simple adiabatic estimation of T_C which is based on a "no strong short-range order" assumption can be questionable and much more sophisticated approaches are required. However, the calculated parameters can be used *mutatis mutandis* in these more elaborated theories.

IV. RESULTS AND DISCUSSION

A. Co_2MnZ (Z=Ga, Si, Ge, and Sn) compounds

To start with, we performed calculations of the electronic band structures of four Co-based Heusler alloys with the generic formula Co_2MnZ (Z=Ga, Si, Ge, and Sn). The results for the electronic spectra are in good agreement with existing calculations of the electronic structures of these compounds.[9–14] To better analyze the density of states (DOS) curves presented later, we first schematically sketch the hybridizations[30] of the minority-spin orbitals between the Co and Mn atoms in Co_2MnGa, given in Fig. 2. It is justified to take the minority-spin orbitals because, due to the exchange hole, these lie higher in energy and are relatively diffuse such that they are much more involved in the chemical bonding.[31] Their larger diffuseness also leads to the finding that spin-polarized ground states show larger interatomic distances despite of having a lower total energy.[32] Compared to the case of Co_2MnGe,[10] the Fermi energy (E_F) in the Z=Ga case (see Fig. 2) is placed below the Co-Co t_{1u} and e_u orbitals. For Co_2MnGe, the t_{1u} orbital is filled with one extra electron.

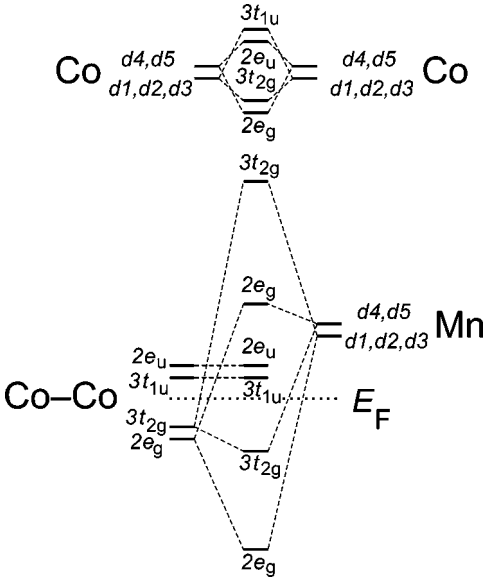

FIG. 2. Schematic hybridization between the minority spin orbitals of Co_2MnGa, first between two Co atoms (top), then between two Co atoms and a neighboring Mn atom (bottom). The coefficients label the degeneracies of the orbital sets (see notations in Ref. 10).

Figure 3 presents the spin-polarized DOS of Co_2MnGa, and the splittings between different symmetry states have

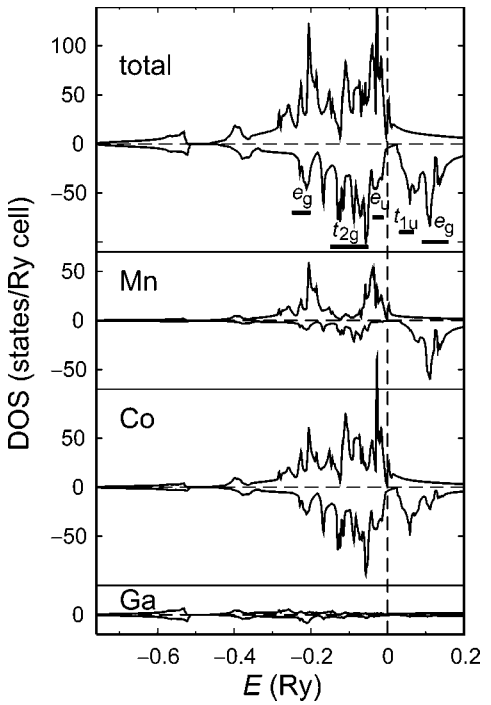

FIG. 3. Total and partial DOS for the compound Co_2MnGa. The character of each peak belonging to the minority spin states has been indicated, and the Fermi level is set to the energy zero.

TABLE II. Sublattices contributions J^0_{nm} (in mRy) to the effective magnetic exchange parameters $J^0_n=\Sigma_m J^0_{nm}$ for the X_2MnZ group of compounds (both LWA and exact adiabatic results are shown).

	X-*X*		*X*-Mn		Mn-Mn	
Compound	J^{lw}	J	J^{lw}	J	J^{lw}	J
Co_2MnGa	−0.36	−0.21	5.8	7.31	0.81	0.89
Co_2MnSi	1.57	2.6	10.2	11.4	1.83	1.85
Co_2MnGe	1.12	2.3	8.92	10.1	2.20	2.2
Co_2MnSn	0.55	0.94	8.66	9.9	2.24	2.3
Rh_2MnGe	0.06	0.2	3.17	4.0	1.28	1.31
Rh_2MnSn	0.11	0.25	3.38	4.25	1.29	1.38
Rh_2MnPb	0.14	0.38	3.24	4.15	1.32	1.35
Ni_2MnSn	−0.064	−0.1	1.92	2.8	2.52	2.63
Cu_2MnSn	0.00	0.01	0.26	0.40	5.71	5.9
Pd_2MnSn	0.00	0.01	0.29	0.41	2.17	2.34

been extracted at the zone center Γ for minority-spin states (see also discussion in Ref. 10). Note that this is an oversimplification because the symmetry labels are not strictly valid over the entire reciprocal space. As expected, the DOS around the Fermi level is heavily dominated by the 3*d* states of the Mn and Co atoms, and the majority spin states are nearly fully occupied. The DOS curves for the minority spins exhibit two peaks above the Fermi level which are due to both Mn and Co 3*d* contributions. The difference in the positions of these two peaks is directly determined by the difference in intra-atomic exchange splitting between Mn and Co. The broad structure in the lowest energy region between −0.8 and −0.55 Ry goes back to (magnetically inactive) 4*s* and 4*p* states of Ga, and they are well separated from the 3*d* states positioned in an energy region between −0.45 and 0.3 Ry. It is interesting to note that the Fermi level of Co_2MnGa is found at the DOS minimum of the minority states, but for Z=Si and Ge it is positioned exactly in a gap, that is, these two latter compounds exhibit 100% spin polarization. This gap has previously been reported by other authors and is formed due to the strong 3*d*-3*d* hybridization (orbital mixing) between the Co and Mn atoms.[13,14]

In such half-metallic compounds the total spin moment should ideally be an integer number (see discussion in Ref. 10). Our results for the Co_2MnZ group, presented in Table I, come very close to that finding, and there is only a slight deviation from integer numbers reproducing so-called Slater-Pauling behavior: here, the total moment equals $\mu_{tot}=N-24$ where N is the total number of valence electrons per unit cell. In accord with the DOS observation in Fig. 3, the Z (*sp*-type) atoms in Co_2MnZ have negligible moments. The minority-spin states of the Mn atoms are nearly empty (see also Fig. 3), and the values of the local Mn spin moments arrive at ca. $3\mu_B$. The Co atoms do have significant spin moments, about $0.7\mu_B$ in Co_2MnGa and about $1.0\mu_B$ in the remaining compounds of this family. Clearly, and also most importantly, the exchange interactions between the Co and Mn atoms cannot be neglected *a priori*.

Accordingly, the calculated values of the partial contributions J^0_{mn} to the effective exchange parameter J^0_n are presented in Table II. As has been alluded to already, the interaction between Mn and Co atoms gives a *leading* contribution to the total effective coupling, thereby questioning the assumption used in earlier work[9] in that only Mn-Mn interactions were taken into consideration; in terms of 3*d*-3*d* orbital overlap, this leading contribution is not at all surprising. On the other side, the Co-Co interaction is negative (−0.36 mRy) in Co_2MnGa and thereby demonstrates the tendency for AFM ordering in the Co sublattice. This negative value, however, is compensated by the larger *positive* interaction between Co and Mn ($J^0_{\text{Co-Mn}}\approx 2\times 2.9$ mRy) such that the *effective* J_0 of Co remains large and positive. The Mn-Mn contribution to J^0_{Mn} is on the order of only 1 mRy, this is nearly five times smaller than the Co-Mn interaction.

For completeness, we mention that pure α-Mn exhibits an AFM ordering at low temperature ($J_0<0$), and the small positive exchange parameters by the nearest-neighbor Mn-Mn pairs in Mn-based Heusler compounds correspond to likewise positive and small second-neighbor pairs exchange parameters in pure α-Mn. The theoretical values for the Curie temperatures T_C obtained by the MFA are also included in Table I. For Co_2MnGa, T_C arrives at 635 K and underestimates the experimental value (694 K) by about 10%. Taking into account the observation that the MFA usually *overestimates* Curie temperatures, this must be considered an even larger disagreement with experiment indicating a presence of magnetic short-range order.[36]

To check the nature of this disagreement, we performed a calculation of J beyond the LWA using Eq. (10). In Table I we also show the corresponding results obtained using this approach. Our calculations reveal that the effective coupling between the Mn atoms is practically unchanged so that the LWA is perfectly suitable for the description of this coupling. However, all other couplings are affected much more strongly by this approximation. For instance, the Co-Co interactions are modified nearly by a factor of 2 while Co-Mn

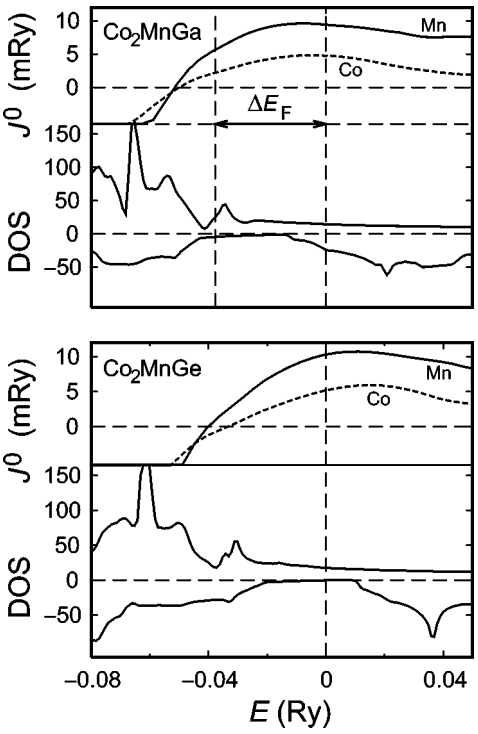

FIG. 4. Density of states and $J^0(E)$ for the Mn (solid line) and Co (dashed line) atoms of Co_2MnGa (top) and Co_2MnGe (bottom). The Fermi level is at zero energy for Co_2MnGe (29 valence electrons) and shifted to the left for Co_2MnGa (28 valence electrons) by the rigid-band shift ΔE_F.

interactions are increased by 25–35 % overall. Correspondingly, the estimated critical temperatures of magnetic phase transition for this group of alloys are increased by 10–20 %, and they are larger than the experimentally observed quantities.

It follows from the results presented in Table II that the substitution of the main-group III element Ga by a main-group IV element such as Si, Ge, or Sn leads to a significant increase of both $J^0_{\text{Co-Mn}}$ and $J^0_{\text{Mn-Mn}}$ values. The modification of $J^0_{\text{Co-Co}}$ for $Z=$Sn is related to the very large volume change relative to $Z=$Ge. However, the variation in the absolute value of $J^0_{\text{Co-Co}}$ is much smaller than the total value of J_0. The implications for the changing electronic structure introduced by the elemental substitution can be well described within the rigid-band approximation (RBA) (see Ref. 10 and 14). For illustration, Fig. 4 shows a comparison between the electronic structures of Co_2MnGa and Co_2MnGe in the energy region ± 0.1 Ry around the Fermi level. The zero energy in the lower DOS curve corresponds to the Fermi level of Co_2MnGe with 29 valence electrons (28 for Co_2MnGa); the Fermi levels are shown by the dashed vertical lines in both DOSs. Despite the fact that the zero energy in Co_2MnGa is not exactly in the gap of the minority spin states (like in Co_2MnGe), the contribution from these additional filled states is small because it reduces the total magnetic moment by $0.3\mu_B$ and slightly changes the position of the $J_0(E)$ extremum in the Ga-based compound. Thus, the RBA reproduces the substitution of Ga by Ge fairly well, at least qualitatively.

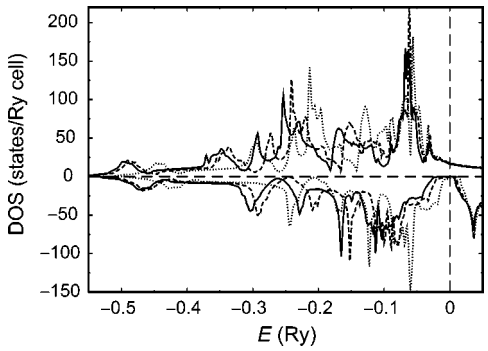

FIG. 5. Density of states of the compounds Co_2MnSi (solid line), Co_2MnGe (dashed line), and Co_2MnSn (dotted line). The Fermi level is at the energy zero.

Nonetheless, the total moment calculated from the electronic structure of Co_2MnGa only by extending the DOS to 29 valence electrons is just $4.6\mu_B$, that is, 8% smaller than the numerical result ($5\mu_B$) for Co_2MnGe, and we will soon focus on this small discrepancy originating from differing interatomic distances. In the frame of the RBA, the significant increase in the exchange parameters (Table II) in going from Co_2MnGa to Co_2MnGe goes back to the shift of the Fermi energy (band filling in Ref. 22) which corresponds to the one extra electron. This evolution of the effective parameters $J^0_{\text{Mn}}=J^0_{\text{Mn-Mn}}+J^0_{\text{Mn-Co}}$ and also $J^0_{\text{Co}}=J^0_{\text{Co-Co}}+J^0_{\text{Mn-Co}}/2$ as a function of the Fermi level is also included in Fig. 4. In fact, the J_0 values of Co_2MnGa at the Fermi level corresponding to Co_2MnGe equal those of the real Co_2MnGe phase. Taking into consideration the usual MFA overestimation of the Curie temperatures, our calculation for Co_2MnGe gives an acceptable agreement (1115 K) with the experimental value of 905 K.

The dependence of the electronic structures and magnetic properties of the Co_2MnZ alloys on the chemical nature of the isoelectronic Z atom has already been discussed in Refs. 10, 11, 14, and 15. We will focus on the DOSs (see Fig. 5) of Co_2MnZ ($Z=$Si, Ge, and Sn) which all display the same valence electron concentration. Not too surprisingly, the DOSs are similar to the preceding one of Co_2MnGa. However, all peaks below the Fermi level move to higher energies with increasing lattice parameters because of the enlarged atomic radii. This results in a smaller overlap between the Mn 3*d* and Co 3*d* orbitals which, in turn, leads to a smaller dispersion of these bands,[11] becoming more atomiclike. As a consequence, the DOS peaks come closer to each other and their amplitudes grow (Fig. 5).

Because the changes in peak positions upon exchanging the Z element is proportional to the change in the lattice parameter, the replacement of Si by Ge has smaller consequences than the replacement of Ge by Sn; in terms of radii (and chemical behavior), Si and Ge are more similar to each other. Thus, the energetic shift in the DOS peaks is more distinct for Co_2MnSn. In agreement with the results of full-potential calculations,[11] the Mn magnetic moment obtained in our TB-LMTO-ASA calculation slightly *increases* in the Si→Ge→Sn series. On the other hand, the Co magnetic moment is *lowered* so that the total magnetic moment is

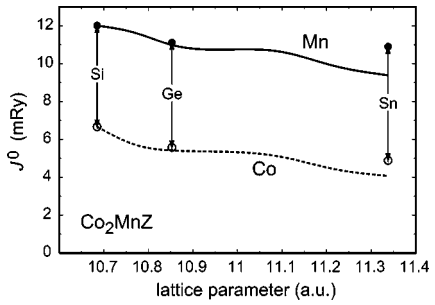

FIG. 6. Course of J^0_{Mn} (solid line) and J^0_{Co} (dashed line) as a function of the lattice parameter in Co_2MnSi. Filled circles correspond to J^0_{Mn} and empty ones to J^0_{Co} for the real Co_2MnZ systems (Z=Si, Ge and Sn) calculated at their experimental lattice parameters.

close to $5\mu_B$ in all three cases (see Table I). This increase of the Mn magnetic moment is consistent with the increase of the Mn-Mn contribution to the effective J_0 (third column in Table II) in this series of compounds. The increase, however, is compensated by lower values for the Co-Co and also Co-Mn interactions. Thus, the calculated T_C's decrease along the line Si→Ge→Sn (see Table I), and this qualitative trend agrees with the tendency observed experimentally.

To fully demonstrate the volume dependence of the exchange interactions (and Curie temperatures, too), we also calculated the course of J_0 in Co_2MnSi *solely* as a function of its volume. That is to say, the structure of Co_2MnSi was artificially expanded to lattice parameters that would better fit the compounds adopted by its higher homologues Ge and Sn; unfortunately, this is impossible to realize experimentally. Figure 6 displays the values of the J_0 parameters obtained from these calculations, and the purely volume-derived exchange parameters exhibit the same tendencies as do the J_0 for the real Co_2MnGe and Co_2MnSn systems with their correct lattice parameters. Nonetheless, the simple calculation based only on the volume change significantly overestimates the decrease of J_0 for Co_2MnSn; the disagreement is a consequence of the differing electronic structures of the Si and Sn atoms. One possible way to imitate this difference is to select a volume for Co_2MnSi which leads to equivalent conduction-electron bandwidths for both compounds, and the necessary lattice parameter for the Si-based alloy is equal to 10.97 a.u. Then, the values of J_0 can be reproduced with an accuracy of a few percents. Summarizing, the decrease of the Curie temperature can be explained by the following two causes: by a simple volume effect and by a change of bandwidth upon substitution.

A detailed comparison of Tables III and IV in terms of J_{ij} makes it clear that the interactions are relatively short ranged and do not exceed the first four neighbors in each sublattice. The main exchange parameter, J_1 of Co_1-Mn in Table III, corresponds to the nearest-neighbor Co-Mn interaction. This particular entry of the table alone already gives about 70% of the total contribution to J_0 between Co and Mn atoms and is about 10 times larger than the corresponding Co-Co and Mn-Mn interactions; a remarkable result but, as has been said before, not too surprising when considering the interatomic overlap. For comparison, Table III also contains the exchange parameters obtained in earlier work[9] where the authors calculated Mn-Mn exchange parameters from the total energy differences of the FM and AFM structures but ignored the Co-Mn interactions.

Naturally, their approach had to result in significantly larger Mn-Mn interactions in order to reproduce the FM/

TABLE III. Pair exchange interaction parameters J_{ij} (in μRy) in the LWA for the Co_2MnZ (Z=Ga, Si, Ge or Sn) family and results from Ref. 9.

Compound	Sublattice	J_1	J_2	J_3	J_4	J_5	J_6	J_7	J_8
Co_2MnGa	Co_1-Co_1	−11	4	−7	−7	2	2	1	1
	Co_1-Co_2	49	4	−76	−5	0	−3	2	1
	Co_1-Mn	557	64	−5	−3	−1	−3	0	0
	Mn-Mn	36	−2	4	17	2	−3	8	3
Co_2MnSi	Co_1-Co_1	5	59	1	1	1	−2	1	1
	Co_1-Co_2	165	72	−31	−6	10	0	2	1
	Co_1-Mn	1106	38	12	2	4	1	0	0
	Mn-Mn	130	58	−12	24	0	−8	0	−2
Co_2MnGe	Co_1-Co_1	−11	55	2	2	1	−2	0	0
	Co_1-Co_2	136	75	−53	−5	10	−1	2	1
	Co_1-Mn	932	41	11	3	6	1	0	0
	Mn-Mn	141	60	−5	23	1	−5	1	−4
Co_2MnSn	Co_1-Co_1	−40	57	4	4	2	−5	0	0
	Co_1-Co_2	73	87	−56	−6	13	−4	2	4
	Co_1-Mn	907	40	7	0	9	2	4	1
	Co_1-Mn	907	40	7	0	9	2	4	1
	Mn-Mn	126	78	5	26	−3	−13	0	0
	Mn-Mn (Ref. 9)	630	135						

TABLE IV. The radius-vector **r**, the distance from the central atom *r*, and the number of equivalent nearest neighbors *n* for the $L2_1$ type of structures.

J_i	X_1-X_1			X_1-X_2			X_1-Mn			Mn-Mn		
	n	*r*	**r**	*n*	*r*	**r**	*n*	*r*	**r**	*n*	*r*	**r**
J_1	12	0.707	$\frac{1}{2}\frac{1}{2}0$	6	0.500	$0\frac{1}{2}0$	4	0.433	$\frac{1}{4}\frac{1}{4}\frac{1}{4}$	12	0.707	$\bar{\frac{1}{2}}\bar{\frac{1}{2}}0$
J_2	6	1.000	$00\bar{1}$	4	0.866	$\bar{\frac{1}{2}}\bar{\frac{1}{2}}\bar{\frac{1}{2}}$	12	0.829	$\bar{\frac{1}{4}}\frac{3}{4}\frac{1}{4}$	6	1.000	$00\bar{1}$
J_3	12	1.225	$\bar{\frac{1}{2}}\bar{\frac{1}{2}}\bar{1}$	4	0.866	$\frac{1}{2}\frac{1}{2}\frac{1}{2}$	12	1.090	$\frac{3}{4}\bar{\frac{1}{4}}\frac{3}{4}$	24	1.225	$\bar{\frac{1}{2}}\bar{\frac{1}{2}}\bar{1}$
J_4	12	1.225	$1\bar{\frac{1}{2}}\bar{\frac{1}{2}}$	24	1.118	$\frac{1}{2}0\bar{1}$	12	1.299	$\frac{5}{4}\bar{\frac{1}{4}}\frac{1}{4}$	12	1.414	$\bar{1}10$
J_5	12	1.414	$\bar{1}10$	6	1.500	$00\bar{\frac{3}{2}}$	4	1.299	$\bar{\frac{3}{4}}\frac{3}{4}\frac{3}{4}$	24	1.581	$0\bar{\frac{1}{2}}\bar{\frac{3}{2}}$
J_6	24	1.581	$0\bar{\frac{1}{2}}\bar{\frac{3}{2}}$	12	1.500	$\bar{1}\bar{\frac{1}{2}}\bar{1}$	24	1.479	$\bar{\frac{5}{4}}\frac{3}{4}\frac{1}{4}$	8	1.732	$\bar{1}\bar{1}\bar{1}$
J_7	4	1.732	$\bar{1}\bar{1}\bar{1}$	12	1.500	$\bar{1}\frac{1}{2}\bar{1}$	12	1.639	$\bar{\frac{3}{4}}\frac{5}{4}\frac{3}{4}$	48	1.871	$\frac{3}{2}1\bar{\frac{1}{2}}$
J_8	4	1.732	$\bar{1}1\bar{1}$	12	1.658	$\frac{1}{2}\frac{3}{2}\frac{1}{2}$	12	1.785	$\frac{1}{4}\bar{\frac{7}{4}}\frac{1}{4}$	6	2.000	$00\bar{2}$

AFM energy differences because in such an approximation all interactions (Mn-Mn and Mn-Co) are effectively *mapped* into the Mn-Mn-type J_{ij}. Thus, one needs to compare an effective parameter for the Mn atom, namely $J^0_{\mathrm{Mn}}=J^0_{\mathrm{Mn-Mn}}+J^0_{\mathrm{Mn-Co}}$ from Table II with $J^0_{\mathrm{Mn}}=12\times J_1+6\times J_2$ from Ref. 9. The obtained values are 10.9 mRy and 8.4 mRy correspondingly. This similarity between the results of the very different models suggests relatively localized magnetic character in this system.

B. Rh_2MnZ (Z=Ge, Sn, and Pb) compounds

Independent full-potential calculations of the electronic structure of this group have been published recently.[10] To ease the understanding of this chemical system, we compare the densities of states of Rh_2MnSn with the preceding one of Co_2MnSn, and both are included in Fig. 7. Generally, the gap in the minority-spin states of the Co_2MnZ phases can also be observed for the Rh_2MnZ phases but this gap apparently becomes broader and the Fermi level is no longer found in the gap. Consequently, the total magnetic moment can no longer be an integer number for this group of intermetallic compounds, and the entries of Table I impressively support this statement.

Another important difference is given by the smaller width and also polarization of the rhodium 4*d* states relative to those of cobalt. In chemical terms, this notable difference between the 3*d* and 4*d* (and also 5*d*) elements is easily explained by differences in spatial shielding, with interesting similarities to main-group chemistry.[31] In any case, the magnetic moment of the Rh atoms is only about one-half the size of those of the Co atoms, namely ca. $0.45\mu_B$ compared to ca. $1\mu_B$.

In contrast to the Co-based system, the Mn moments in this group are larger by about $0.6\mu_B$. Such a change has been explained[10] by a smaller hybridization between the Rh and Mn atoms than between the Co and Mn atoms. Alternatively, a chemical interpretation would focus on an effectively oversized Mn atom because of the strongly widened lattice due to the large Rh atoms. Thus, the majority/minority spin splitting for Mn is strongly favored, and the intra-atomic exchange splitting will be mirrored by extraordinarily diffuse minority-spin orbitals for Mn. The same effect takes place in $FePd_3$ where Fe acquires a very large moment because of being too spacious.[31] Unlike the results given in Ref. 10, however, the total magnetic moments of our calculations do not monotonically increase in the row Ge→Sn→Pb, but this effect is probably related to the atomic spheres approximation used by us.

We will now analyze the results for the exchange coupling using Eq. (9). The values of the exchange splittings m_iI_i for the Rh atoms are about three times smaller than for the Co atoms so that Rh-Rh and Rh-Mn exchange parameters are about 10 and three times lower if compared with the Co-Co and Co-Mn pairs (see Table II) only because of this splitting renormalization. Such a simple explanation, however, is not

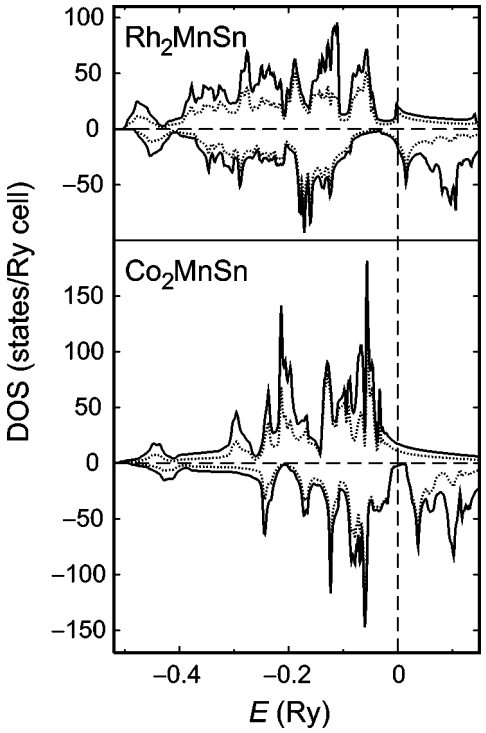

FIG. 7. Total (solid line) and partial densities of states (dashed line) of Rh and Co in Rh_2MnSn and Co_2MnSn. The Fermi level is at the energy zero.

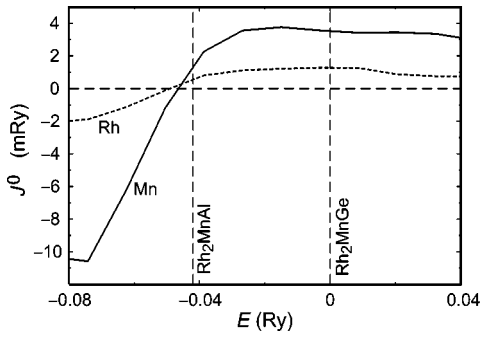

FIG. 8. The calculated effective exchange parameters J^0_{Mn} (solid) and J^0_{Rh} (dashed line) as a function of band filling for Rh_2MnGe. Vertical lines corresponds to 28 (Rh_2MnAl) and 29 (Rh_2MnGe) electrons per unit cell. The energy zero corresponds to the Fermi level of Rh_2MnGe.

applicable for the Mn-Mn interactions where the corresponding susceptibility has also changed. In the Mn sublattice, the interactions decrease in magnitude by about 1 mRy upon substitution of Co by Rh despite the increase visible for the Mn magnetic moments. The lowered Mn-Mn exchange parameters reflect a general AFM tendency for a nearly half-filled *d* band and an FM tendency for a nearly empty or filled *d* band; this has been discussed before.[33] The manganese *d* states in the Rh-based compounds are nearly half-filled while in Co-based compounds these Mn-centered states have been filled by approximately 0.6 electrons despite Co/Rh being isoelectronic (the *d* states contribution to the magnetic moment of the Mn atoms is $3.7\mu_B$ in Rh_2MnSn and $3.1\mu_B$ in Co_2MnSn).

When it comes to the volume dependence of the magnetic properties of the Rh-based compounds, we reiterate the course found for the Co_2MnZ (Z=Si, Ge, Sn) group (Fig. 5). One also expects a decrease of the Curie temperatures with increasing volume, and this is what the experimental T_C values reflect in the row Ge→Sn→Pb (see Table I). Unfortunately, this trend is somewhat obscured in the theoretical data. The calculated Curie temperatures in the LWA for Rh_2MnSn (435 K) and Rh_2MnPb (423 K) are not too far away from the experimental ones, 412 and 338 K, respectively. For Rh_2MnGe, however, we underestimate T_C (410 K) compared to an experimental 450 K. The usage of Eq. (10) leads to a significant modification of Rh-Rh coupling (factor of 2–3) and a 25–30 % increase of the Rh-Mn coupling, i.e., the MFA produces significantly larger numbers for T_C. However, all relative trends remain similar to the exchange coupling within the LWA.

The energy dependence of J in the Rh_2MnZ compounds, depicted in Fig. 8, looks different from the one discussed before in the Co_2MnZ group. First, the amplitude of $J(E)$ is smaller and, second, the maximum of the curve is a broad plateau. The last finding means that an increase of the electron concentration will *not* lead to a significant change for the exchange parameters. An alternative decrease of the electron concentration, however, leads to negative J values such that an FM state is no longer stable. For instance, the substitution of Ge by Al shifts the Fermi level down by 0.04 Ry (vertical line in Fig. 8) and leads to a significant decrease of J. This interpretation is supported by the experimental AFM ordering observed for Rh_2MnAl.[34]

Closing this section, we would like to mention that the Rh_2MnZ compounds are traditionally discussed as systems with fully localized magnetic moments, in contrast to the Co_2MnZ-type compounds where the Co magnetic moment can obviously not be neglected. The results for the effective J values in Table II and the pair-magnetic exchange values J_{ij} in Table V clearly evidence that Rh-Mn interactions are even *larger* than Mn-Mn interactions. A similar behavior is known from Fe/Pd alloys where the Fe atom magnetically polarizes the 4*d* metal upon strong Fe-Pd chemical bonding.[31] In the present case, the Rh-Mn exchange parameters are mostly determined by the first-neighbor J_1 interaction. Mn-Mn interactions show a significantly longer range with the main contributions coming from large and positive J_1, J_2 and negative J_6 entries.

TABLE V. Pair magnetic exchange interactions J_{ij} (in μRy) in the LWA calculated for Rh_2MnZ (Z=Ge, Sn or Pb).

Compound	Sublattice	J_1	J_2	J_3	J_4	J_5	J_6	J_7	J_8
Rh_2MnGe	Rh_1-Rh_1	−9	13	0	0	−1	0	0	0
	Rh_1-Rh_2	17	0	−3	−2	6	0	0	1
	Rh_1-Mn	312	21	2	2	2	1	0	−1
	Mn-Mn	87	102	3	18	−5	−27	−4	−9
Rh_2MnSn	Rh_1-Rh_1	−8	15	0	0	−2	0	0	0
	Rh_1-Rh_2	20	2	−3	−2	8	−1	0	1
	Rh_1-Mn	340	20	3	2	2	1	1	−1
	Mn-Mn	61	108	6	29	−6	−27	−4	−3
Rh_2MnPb	Rh_1-Rh_1	−8	15	0	0	−2	1	−1	−1
	Rh_1-Rh_2	22	2	−5	−2	7	−1	0	1
	Rh_1-Mn	327	17	5	2	1	1	1	−1
	Mn-Mn	57	96	21	33	−8	−34	−9	−4

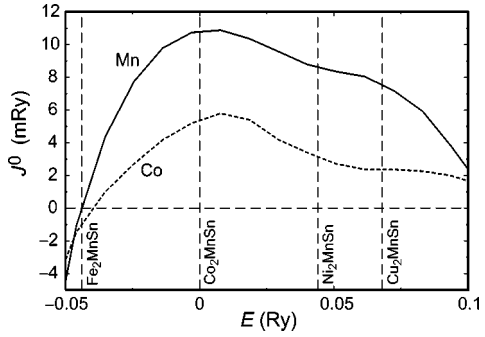

FIG. 9. The calculated effective parameters J^0_{Mn} (solid line) and J^0_{Co} (dashed line) as a function of band filling in Co_2MnSn. Vertical lines correspond to 27 (Fe_2MnSn), 29 (Co_2MnSn), 31 (Ni_2MnSn), and 33 (Cu_2MnSn) electrons per unit cell.

C. X_2MnSn (X=Ni, Cu, and Pd) compounds

In this section, we will analyze the change of the magnetic properties of the Heusler alloys upon atomic substitution by the X component, the non-Mn d metal. For the compounds with X=Ni, Cu, and Pd, the electronic structures have been studied in Refs. 10 and 9. Similar to the preceding Rh_2MnZ group, the Fermi level is no longer in the minority-spin DOS gap and the total moment is not an integer number. The substitution of Co by Rh or Ni leads to a significant decrease of the d-metal polarization and, also, to a nearly complete filling of their minority-spin states. The magnetic moment of the X atoms is thereby reduced from $1\mu_B$ (Co) to ca. $0.5\mu_B$ (Rh) and, finally, to about $0.2\mu_B$ (Ni), given in Table I. This reduction is accompanied by an increase of the Mn magnetic moment only during the first substitution. The limiting case is given by the compounds with the nonmagnetic Cu and Pd atoms.

Using the calculated magnetization values m_i, we can estimate the reduction of the J^0_{X-X} and $J^0_{X-\mathrm{Mn}}$ parameters (see discussion above). The obtained parameters give qualitative agreement with the directly calculated results, listed in Table II. However, this estimation cannot reproduce the decrease of $J^0_{\mathrm{Mn-Mn}}$ for X=Rh and, on the other hand, the significant increase for X=Cu. The authors of Ref. 9 suggested that the principal role of the X atoms is to simply determine the size of the crystal lattice. To check this assumption, we calculated J_0 for Ni_2MnSn but with a lattice parameter that is characteristic for Cu_2MnSn. As a result, $J^0_{X-\mathrm{Mn}}$=1.3 mRy and $J^0_{\mathrm{Mn-Mn}}$=2.3 mRy differ from the correctly calculated J_0 of the real Cu_2MnSn phase by 0.3 and 5.7 mRy, respectively (see Table II). Also, the modified exchange parameters upon d-metal substitution is not reproduced by the RBA which worked nicely for an sp-component substitution.

In order to analyze the problem in more detail, we show the course of $J(E)$ as a function of Co_2MnSn band filling in Fig. 9. The vertical lines correspond to the Fermi levels where the total number of valence electrons is equal to the corresponding compound of the X_2MnSn family. While it is clear that J continuously decreases upon Co→Ni (and also Cu) substitution, this lowering is *underestimated*, and the effective J^0_{Mn} obtained from Fig. 9 is close to 8 mRy but the properly calculated J^0_{Mn} is 5 mRy (see Table II).

The predicted Curie temperatures obtained from the calculated parameters are presented in Table I. The correct tendency for the calculated Curie temperatures has been mentioned above, except for Ni_2MnSn where the disagreement is within the accuracy of the method. The total exchange parameter J_0 is mostly determined by the first X-Mn pair interaction and has significant long-range contributions; at least six interactions are important, see Table VI. We also include the results obtained from total-energy calculations[9] and from a fit to spin-wave dispersions.[16] The exchange coupling in the LWA produces somewhat smaller values for the Mn-Mn interaction while X-Mn interactions are underestimated by 50–60 % when compared with those from the general definition [Eq. (10)]. All T_C's are overestimated in this approach and we expect that any improvement of the MFA will produce better agreement with experiment. The calculated exchange parameters can be used in any more sophisticated calculations of the critical temperature.

As mentioned before, one may compare the Mn total exchange only. The J_{ij} obtained in Ref. 9 are in good agreement with our results for Pd_2MnSn (2.1 and 2.5 mRy, respectively), but for the Ni- and Cu-based compounds, the authors

TABLE VI. Pair magnetic exchange interactions J_{ij} (in μRy) in the LWA calculated for X_2MnSn (X=Ni, Cu or Pd) and results from Refs. 9 and 16.

Compound	Sublattice	J_1	J_2	J_3	J_4	J_5	J_6	J_7	J_8
Ni_2MnSn	Ni_1-Mn	263	−18	1	4	8	1	1	2
	Mn-Mn	151	116	29	−104	14	−30	12	−14
	Mn-Mn (Ref. 9)	187	−13						
	Mn-Mn (Ref. 16)	82	105	38	37	−6	17	4	2
Cu_2MnSn	Cu_1-Mn	30	2	0	0	−1	0	0	0
	Mn-Mn	491	318	−118	19	−12	65	9	9
	Mn-Mn (Ref. 9)	88	97						
Pd_2MnPb	Pd_1-Mn	40	−3	0	0	2	0	0	0
	Mn-Mn	65	116	51	−78	20	−64	16	−5
	Mn-Mn (Ref. 9)	187	−20						
	Mn-Mn (Ref. 16)	64	43	21	−44	14	−19	4	−6

obtained numbers which are two to three times smaller than ours. The result obtained from spin-wave dispersions in Ni_2MnSn (3.3 mRy) is fairly close to our 4.4 mRy but for Pd_2MnSn, however, the disagreement is significant (1.3 versus 2.5 mRy). Nonetheless, it must be mentioned that both calculations of exchange parameters did *not* include the Mn-*X* interactions which are important especially in the Ni_2MnSn system. The results obtained from the energy differences of FM and AFM ordered structures tend to give systematically underestimated exchange parameters although these systems are considered localized-moment systems. The results from spin-wave analysis also underestimate the exchange coupling. We therefore plan to consider the spin-wave properties in future publications.

V. CONCLUSION

The electronic structures and magnetic exchange interactions have been calculated for a set of full-Heusler alloys with generic formula X_2MnZ where *X* is a transition-metal atom and *Z* is an *sp* main-group element. The alloy variations of the Curie temperatures calculated in the mean-field approximation are in good agreement with experimental data. Our analysis demonstrates that the J_{ij} dependence on the *Z* atom may be described within a rigid band approximation, having straightforward implications for the influence of the atomic volume of *Z*, thereby allowing semi-quantitative predictions. The substitution of an *X* element, however, poses a problem for the rigid-band approximation although qualitative tendencies can be identified; for obtaining quantitative results, a full calculation has to be performed. The magnetic exchange parameters and also Curie temperatures decrease along the row $Cu \rightarrow Ni \rightarrow Rh \rightarrow Pd$, in agreement with the degree of *d* localization for the transition metal. The *X*-Mn interactions are very important for systems with sizable magnetic moments on the transition metal (Co, Rh, and Ni), making the magnetic short-range order effects stronger in these materials. The *X*-Mn interactions are limited by first neighbors while Mn-Mn interactions are quite long ranged.

ACKNOWLEDGMENTS

This work was carried out, in part, at Ames Laboratory, which is operated for the U.S. Department of Energy by Iowa State University under Contract No. W-7405-82. This work was supported by the Director for Energy Research, Office of Basic Energy Sciences of the U.S. Department of Energy. The support by Deutsche Forschungsgemeinschaft (Grant No. DR 342/7-1) is also gratefully acknowledged.

[1] R. de Groot and P. van Engen, Phys. Rev. Lett. **50**, 2024 (1983).
[2] S. Ishida, T. Masaki, S. Fujii, and S. Asano, Physica B **245**, 1 (1998).
[3] M. Julliere, Phys. Lett. **54A**, 225 (1975).
[4] J. S. Moodera, L. R. Kinder, T. M. Wong, and R. Meservey, Phys. Rev. Lett. **74**, 3273 (1995).
[5] B. Dieny, V. S. Speriosu, S. S. P. Parkin, B. A. Gurney, D. R. Wilhoit, and D. Mauri, Phys. Rev. B **43**, 1297 (1991).
[6] O. Heusler, Ann. Phys. (Leipzig) **19**, 155 (1934).
[7] Y. Ishikawa, Physica B **91**, 130 (1977).
[8] A. Hamzić, R. Asomoza, and I. A. Campbell, J. Phys. F: Met. Phys. **11**, 1441 (1981).
[9] J. Kübler, A. R. Williams, and C. B. Sommers, Phys. Rev. B **28**, 1745 (1983).
[10] I. Galanakis, P. H. Dederichs, and N. Papanikolaus, Phys. Rev. B **66**, 174429 (2002).
[11] S. Picozzi, A. Continenza, and A. J. Freeman, Phys. Rev. B **66**, 094421 (2002).
[12] A. Ayuela, J. Enkovaara, K. Ullakko, and R. M. Niemenen, J. Phys.: Condens. Matter **11**, 2017 (1999).
[13] S. Fujii, S. Ishida, and S. Asano, J. Phys. Soc. Jpn. **64**, 185 (1995).
[14] S. Ishida, S. Fujii, S. Kashiwagi, and S. Asano, J. Phys. Soc. Jpn. **64**, 2152 (1995).
[15] S. Fujii, S. Sugimura, S. Ishida, and S. Asano, J. Phys.: Condens. Matter **2**, 8583 (1990).
[16] Y. Noda, and Y. Ishikawa, J. Phys. Soc. Jpn. **40**, 690 (1976).
[17] P. J. Webster, Contemp. Phys. **10**, 559 (1969).
[18] Y. Kurtulus and R. Dronskowski, J. Solid State Chem. **176**, 390 (2003).
[19] O. K. Andersen, Phys. Rev. B **12**, 3060 (1975).
[20] O. K. Andersen and O. Jepsen, Phys. Rev. Lett. **53**, 2571 (1984).
[21] S. H. Vosko, L. Wilk, and M. Nusair, Can. J. Phys. **58**, 1200 (1980).
[22] M. van Schilfgaarde and V. P. Antropov, J. Appl. Phys. **85**, 4827 (1999).
[23] *Magnetism of Metals and Alloys*, edited by M. Cyrot (North-Holland, Amsterdam, 1982).
[24] V. P. Antropov, J. Magn. Magn. Mater. **262**, L193 (2003).
[25] V. P. Antropov, in *Computer Simulation Studies in Condensed-Matter Physics XVI*, edited by D. P. Landau (Springer-Verlag, Berlin, Heidelberg, 2003), Vol. 95, p. 41.
[26] J. Callaway, C. S. Wang, and D. G. Laurent, Phys. Rev. B **24**, 6491 (1981).
[27] A. L. Lichtenstein, M. I. Katsnelson, and V. A. Gubanov, J. Phys. F: Met. Phys. **14**, L125 (1984).
[28] V. P. Antropov, B. N. Harmon, and A. N. Smirnov, J. Magn. Magn. Mater. **200**, 148 (1999).
[29] A. Aharoni, *Introduction to the Theory of Ferromagnetism* (Oxford University Press, New York, 1996).
[30] Here we stick to the physics jargon in that "hybridization" means what chemists would call "orbital interaction," not to be confused with a unitary transformation into another set of nonorthogonal but localized orbitals.
[31] G. A. Landrum and R. Dronskowski, Angew. Chem., Int. Ed. **39**, 1560 (2000).

[32] R. Dronskowski, Adv. Solid State Phys. **42**, 433 (2002).
[33] V. P. Antropov, M. I. Katshelson, and A. I. Liechtenstein, Physica B **237–238**, 336 (1997).
[34] H. Masumoto and K. Watanabe, J. Phys. Soc. Jpn. **32**, 281 (1972).
[35] P. J. Webster and K. R. A. Ziebeck, in *Alloys and Compounds of d-Elements with Main Group Elements, Part 2*, edited by H. R. J. Wijn, Landolt-Börnstein, New Series, Group III, Vol. 19/c (Springer, Berlin, 1988), pp. 75–184.
[36] V. P. Antropov, cond-mat/0411393 (unpublished).